Nuclear Science and Techniques (2025) 36:48
https://doi.org/10.1007/s41365-024-01624-w

Plate spent fuel burnup measurement equipment based on a compact D-D neutron generator

Yi-Nong Li[1] · Zheng Wei[1,2,3] · Gen-Tao Gao[4] · Lu Wu[4] · Kang Wu[1] · Jun Ma[1] · Xing-Yu Liu[5] · Ze-En Yao[1,2,3] · Yu Zhang[1,2] · Jun-Run Wang[1,2] · Xiao-Dong Su[1,2] · Zhi-Yong Deng[1,4] · Guo-Rong Wan[4]

Received: 20 February 2024 / Revised: 26 April 2024 / Accepted: 8 May 2024 / Published online: 31 January 2025

Abstract
Burnup measurement is crucial for the management and disposal of spent fuel. The conventional approach indirectly estimates burnup by examining the fission product or actinide content. Compared to the first two methods, the active neutron method exhibits a lower dependence on the irradiation history and initial enrichment degree of the spent fuel. In addition, it can be used to directly determine the content of fissile nuclides in spent fuel. This study proposed the design of a burnup measurement equipment specifically crafted for plate segments by utilizing a compact D-D neutron generator. The equipment initiates the fission of fissile nuclides within the spent fuel plate segment through thermal neutrons provided by the moderators. Subsequently, the burnup is determined by analyzing the transmitted thermal neutrons and counting the fission fast neutrons. The Monte Carlo program Geant4 was used to simulate the relationship between spent fuel plate segment assembly burnup and the detector count of 10 MW material test reactor designed by the International Atomic Energy Agency. Consequently, the feasibility of the method and rationality of the detector design were verified.

Keywords Burnup measurement · Plate spent fuel · Active neutrons

1 Introduction

With the development of nuclear energy and technology, the efficient utilization of nuclear energy, particularly in the form of a plate fuel assembly (PFA), has emerged as a prominent international research focus. Compared with the traditional rod fuel assembly, the PFA exhibits a denser structure, enhanced coolant utilization efficiency, and superior economic and safety performance relative to a rod spent fuel assembly of equivalent size. The increased core density of plate fuel reactors facilitates a greater neutron flux. This has prompted extensive investigations into plate fuel reactors, such as the International Atomic Energy Agency (IAEA) 10 MW material test reactor [1–3], Japan's JRR-3 and JRR-4 reactors [4], and China's Advanced Research Reactor (ARR) [5]. These studies have explored the anti-irradiation effects of materials and reactor characteristics, and underscored the advancements in this field. However, there is a dearth of research on the burnup measurement of spent fuel within a plate fuel assembly.

Burnup measurement is a pivotal technology in spent fuel treatment and disposal and constitutes a central aspect of

This work was supported by the National Natural Science Foundation of China (No. 12075105), the Major Science and Technology Projects of Gansu Province (No. 22ZD6GB020), the NSFC-Nuclear Technology Innovation Joint Fund (No. U2167203), and the Fundamental Research Funds for the Central Universities (lzujbky-2023-stlt01, lzujbky-2024-jdzx10).

✉ Zheng Wei
weizheng@lzu.edu.cn

1 School of Nuclear Science and Technology, Lanzhou University, Lanzhou 730000, China

2 Engineering Research Center for Neutron Application, Ministry of Education, Lanzhou University, Lanzhou 730000, China

3 Frontiers Science Center for Rare Isotopes, Lanzhou University, Lanzhou 730000, China

4 Nuclear Power Institute of China, Chengdu 610000, China

5 Wuhan Second Ship Design and Research Institute, Wuhan 430205, China

nuclear security. Burnup in spent fuel delineates the total energy produced per unit mass of nuclear fuel loaded into the core, serving as an indicator of fuel depletion, expressed in MW·d/tHM or percentage depletion. Burnup can be measured using destructive analysis or nondestructive testing methods [6]. Although destructive analysis ensures high measurement accuracy, its large-scale application in nuclear facilities beyond research facilities is challenging because of the strong radioactivity of spent fuel and the intricacies of the analysis process.

Presently, the internationally recognized nondestructive testing methods for burnup primarily include passive neutron measurement and the gamma detection method [7–10]. Passive neutron measurement entails the detection of spontaneous fission neutron emissions from actinides in spent fuel to assess the burnup. The nuclides commonly used for passive neutron detection are ^{242}Cm and ^{244}Cm, which are formed from ^{235}U or ^{238}U after multiple neutron captures and exhibit a power-exponential relationship with burnup. Spent fuels with the same burnup albeit different irradiation histories differ in terms of neutron emissivity by less than 10%. In addition, passive neutron detection is less affected by the spent fuel cooling time, with passive neutron emissions from spent fuel reduced by less than 50% over a 30-year period [11]. However, passive neutron measurements require a highly accurate measurement position, and the moderator concentration in the measurement tank must be corrected [12–14].

Currently, gamma detection is the most widely used method for burnup detection. It offers the advantages of a short measurement period, simple operation, and burnup measurement of the entire spent fuel assembly. Its measurement principle detects the photon energy spectrum emitted by the spent fuel. Finally, the burnup value of the fuel to be measured is obtained from the relationship between the nuclides and burnup. The nuclides used for the gamma spectrum analysis are referred to as labeling nuclides. The commonly used labeling nuclides are generally fragment nuclides with long half-lives, such as ^{106}Ru, ^{134}Cs, ^{137}Cs, ^{144}Ce,^{154}Eu, ^{125}Sb, etc [15–20]. Burnup can be solved by establishing the ratio relationship between nuclides and burnup, which is highly dependent on the initial enrichment degree and irradiation history of the fuel, particularly when measuring the burnup of low-enriched uranium with deep burnup. Because of the difference between the fissionable element yield of ^{239}Pu generated by irradiation and the initial fissionable nuclide ^{235}U, the equation must be modified accordingly. In addition, the use of long half-life labeling nuclides to measure the burnup of fuels with complex irradiation histories introduces large uncertainty because of cumbersome data processing.

Both methods have merits and drawbacks because they rely on the irradiation history and initial enrichment information of the fuel assembly [21]. In recent years, burnup measurement methods have attracted increasing attention in various countries [22–27]. Burnup measurement methods based on active neutron challenge technology have been widely studied [28–31]. Compared with passive neutron and gamma measurements, the active neutron method enables the direct measurement of the remaining fissile nuclide content within the spent fuel, independent of the irradiation history or initial enrichment.

In this study, an equipment was proposed to measure the burnup of a plate spent fuel assembly by utilizing a D-D neutron generator. The 2.45 MeV neutrons emitted by the D-D neutron generator were moderated by thermal or epithermal neutrons. Subsequently, fission neutrons were generated by inducing fission in fissile nuclides within the spent fuel assembly. The burnup was quantified by detecting neutron counts using a "U-shaped" neutron detector.

The plate segment fuel assembly from the IAEA10MW material test reactor served as the reference assembly for this study. The moderator structure and detector configuration were simulated and optimized using Monte Carlo simulation software Geant4 [32, 33]. The fission process was simulated using the FTFP_BERT_HP physical model provided by Geant4. Consequently, the burnup-count relationship for the spent fuel assembly under various burnup scenarios was obtained.

2 MTR fuel assembly

The 10MW material test reactor (MTR) is an idealized pool material test reactor designed by the International Atomic Energy Agency and is used to compare calculation methods and codes in terms of safety-related aspects. The MTR is a pool reactor that uses two different enriched and sized fuel assemblies: high-enriched fuel containing 93% enriched uranium and low-enriched fuel containing 20% enriched uranium. The MTR uses a considerable amount of light water as a peripheral reflector, and the neutron scattering response is relatively anisotropic [34].

The MTR core comprises 24 standard-size fuel assemblies and 2 half-size fuel assemblies and 4 control assemblies in an approximately 5×6 matrix arrangement. Each fuel element and graphite element has an axial reflector with a volume fraction of 20% Al and 80% H_2O at each end. Further, it has a H_2O reflective layer with a thickness of 150 mm on the outer side [34–36].

The burnup parameter information was derived from the 10MW segment fuel data sourced from IAEA-TEC-DOC-233 [36]. The considered nuclides include ^{235}U, ^{236}U, ^{238}U, ^{239}Pu, ^{240}Pu, ^{241}Pu, and ^{242}Pu. The fission products considered were ^{135}Xe and ^{149}Sm. The variation in the individual nuclides with burnup is shown in Fig. 1.

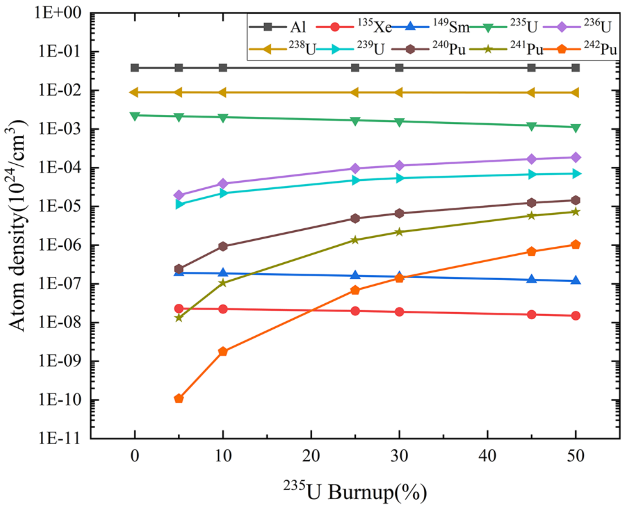

Fig. 1 (Color online) Burnup-nuclide relationship

3 Plate spent fuel burnup measurement system

The layout of plate spent fuel burnup measurement system is shown in Fig. 2. The system comprised four main components: a compact D-D neutron generator, neutron moderator, slab fuel assembly, and "U-shaped" ^{3}He neutron detection system.

As shown on the left-hand side of Fig. 2, the outside of the compact D-D neutron generator was wrapped with HDPE (yellow part in Fig. 2) and fixed to the support bracket (orange in Fig. 2). The neutron moderator comprised three parts: HDPE at the front (yellow part in Fig. 2), D_2O at the back (blue part in Fig. 2) and graphite wrapped in the outer layer (brown part in Fig. 2). The right side of Fig. 2 shows a U-shaped ^{3}He neutron detection system comprising fission neutron detectors on both sides and a transmission neutron detector on the back. The two-sided neutron detectors were composed of HDPE support and ^{3}He neutron detectors with Cd sheets at the front. The back-transmission neutron detector comprised an aluminum support and ^{3}He detectors.

The compact D-D neutron generator served as the neutron source, providing exogenous neutrons. These neutrons, with an energy of 2.45 MeV, were moderated into thermal or epithermal neutrons using the neutron moderator. Moderated neutrons interacted with the fuel assembly to produce fission neutrons or were absorbed or scattered by nuclides in the assembly.

The "U-shaped" ^{3}He neutron detection system measured the neutron intensity on the arms and backs of the spent fuel assembly. The neutron intensities of fuel assemblies were measured using a neutron moderator. Burnup measurements using the neutron count rates from the "U-shaped" ^{3}He neutron detection system arms and backs contribute to determining the average burnup of the spent fuel assembly. A response model correlating the neutron intensity with the burnup of the spent fuel assembly of the plate was established using a Monte Carlo simulation.

Fig. 2 (Color online) Layout of plate spent fuel burnup measurement system

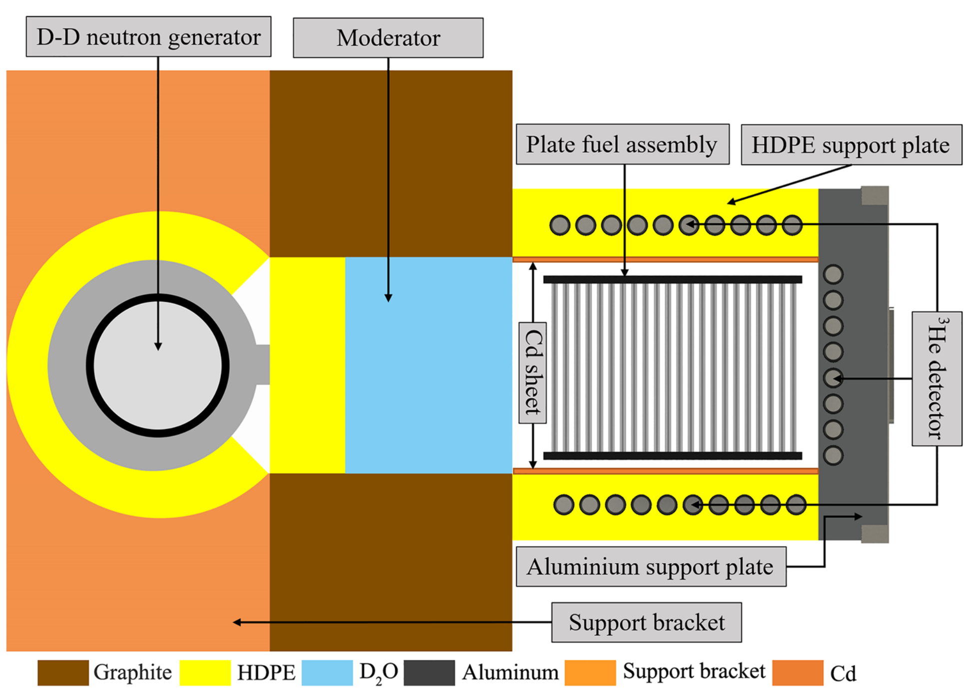

4 Detector physical design

4.1 D-D neutron generator

A compact D-D neutron generator developed by Lanzhou University was used as an external neutron source [37–40]. The specific structures are shown in Fig. 2. The compact D-D neutron generator comprised four main components: the main body of the neutron generator, power supply and control integration cabinet, cooling cycle system, and industrial control machine.

When the neutron generator is in operation, the deuterium ion beam generated by the ionization of the dual plasma sources is accelerated to bombard the deuterium-titanium target under the action of an external high-voltage electric field. Consequently, the D-D fusion nuclear reaction occurs, generating quasi-monoenergetic fast neutrons with an energy of approximately 2.45 MeV. A neutron generator can provide a stable neutron beam current of greater than 5×10^8 nps with beam fluctuations of less than 3% [38].

4.2 Neutron moderators

The primary nuclide in the spent fuel assembly was ^{238}U, which constituted approximately 56.7% of the spent PFA. However, the active neutron interrogation method for measuring burnup targets the nuclides ^{235}U and ^{239}Pu. ^{238}U is a fissile nuclide with a fission cross-section in the thermal neutron energy region of only approximately 10^{-3} barn. However, it undergoes resonant absorption by ^{238}U at neutron energies of 10 eV or more, potentially affecting the measurement accuracy. As shown in Fig. 3, ^{238}U and ^{239}Pu are fissile nuclides with reaction cross sections of approximately 1000 barn in the thermal neutron energy region. With an increase in neutron energy, the fission cross sections of ^{238}U, ^{235}U, and ^{239}Pu gradually converge. When the neutron energy is greater than 1 MeV, the difference between the three fission cross sections is only two orders of magnitude.

Considering this, to mitigate the influence of the ^{238}U nuclide on the active neutron burnup measurements, it is necessary to moderate 2.45 MeV fast neutrons to thermal neutrons with energies lower than 10 eV. The moderator was designed with the goal of achieving a thermal neutron ratio of not lower than 70% while maximizing the injection of thermal neutrons. This design approach aimed to enhance the accuracy and reliability of burnup measurements by considering the specific characteristics and interactions of different fissile nuclides in the PFA.

Based on comprehensive material moderating effects, physical properties, and price considerations [41], Geant4

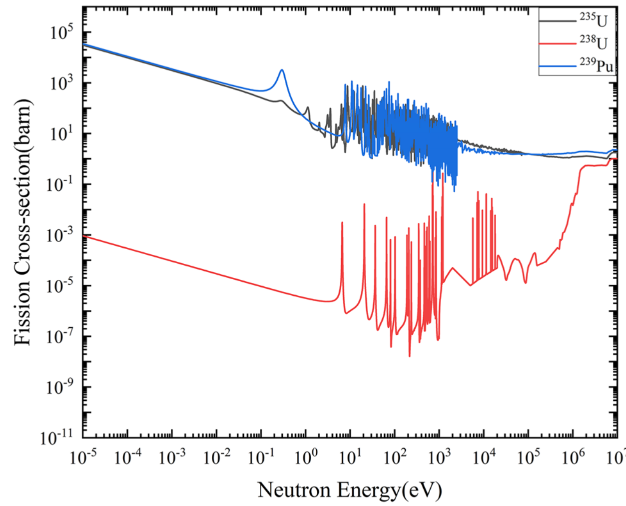

Fig. 3 (Color online) Fission cross sections of ^{235}U, ^{238}U, and ^{239}Pu

was used to establish the model. The overall cross section of heavy water (D_2O) and polyethylene (PE) Was 250 mm × 250 mm. Heavy water was encased in aluminum, with the aluminum shell at the bottom being 1 mm thick, and the aluminum shells on the side and top measuring 3 mm thick. To enhance the neutron utilization efficiency, a 300-mm reflective layer of polyethylene was added to the side and back of the neutron generator. In addition, the moderator was enveloped with 250-mm graphite, which served as the primary neutron moderator. An additional 250-mm layer of graphite was used as the neutron reflection and auxiliary moderating material. This layer was designed to scatter a portion of the neutrons, thereby allowing them to return to the moderator for continued moderation. The purpose was to minimize the neutron transmission and maximize the interaction of neutrons in the moderator, which achieves a better slowing effect.

A neutron detector was added into the end of the moderator in Geant4 model (not shown in Fig. 2). This detector was crucial for capturing and analyzing the neutron spectrum resulting from interactions within moderator materials. Through simulations and analyses using the Geant4 program, the performance and efficiency of the designed moderator system were evaluated to ensure that it satisfied the desired requirements for thermal neutron spectrum generation. To determine the thickness of the neutron moderator, the neutron-moderating effects of PE and D_2O were simulated using Geant4.

In Fig. 4a, the neutron flux exhibited a rising and then decreasing trend with an increase in the polyethylene (PE) thickness. The thickness of the first layer of the moderator, 75 mm, was chosen as the point of the highest neutron flux. At this thickness, the neutron flux was $7.04 \times 10^{-5}\ \mathrm{n/cm^2s^{-1}}$ (per unit source neutron), and the proportion of thermal

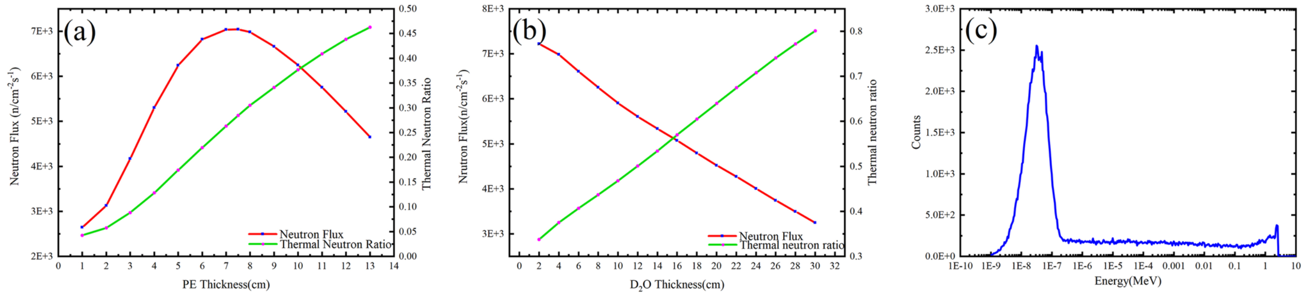

Fig. 4 (Color online) Relationship between moderator thickness and thermal neutrons. **a** Variation of neutron injection rate with PE thickness. **b** Variation of neutron injection rate with D_2O thickness. **c** Moderated neutron spectrum

neutrons was 28.50%. Once the thickness of the first layer (75 mm PE) was determined, a simulation was performed to determine the thickness of the second layer, as shown in Fig. 4b.

With an increase in heavy water (D_2O) thickness, the thermal neutron percentage gradually increased, whereas the neutron injection rate decreased. Considering the neutron injection rate, thermal neutron ratio, equipment size, and material cost, the thickness of the second D_2O layer was obtained as 260mm. At this thickness, the neutron flux was 3.73×10^{-5} n/cm^{2}s^{-1} (per unit source neutron), and the thermal neutron ratio was 74.1%. Figure 4c depicts the D-D moderated neutron spectrum under the moderator conditions. The overall size of the moderating body was 750 mm × 750 mm × 350 mm.

4.3 "U-shaped" detector structure

The "U-shaped" ^{3}He neutron detector system comprised two main components: an arm neutron detector and a back-neutron detector. This system was designed to detect neutrons emitted from a plate-shaped spent fuel assembly. The structure of the detector system is shown in Fig. 2.

The back-neutron detector was responsible for detecting transmission neutrons that passed through the spent fuel assembly without reacting. It comprised two high-density polyethylene (HDPE) support plates and an aluminum alloy support plate. A total of 22 ^{3}He counting tubes were embedded into the support plates. The structure of the back detector was optimized to capture the transmitted neutrons. Aluminum alloy was chosen as the back component because of its small thermal neutron absorption cross section, which helps avoid interference with transmitted neutrons.

The arm-neutron detector was designed to detect fission neutrons resulting from the induced fission of the spent fuel assembly. The primary material of the arm was HDPE. HDPE can moderate fast neutrons generated from fission while also functioning as a shield to protect against scattered neutron interference in the surrounding environment. This is essential for accurate and reliable detection of neutrons.

The "U-shaped" hollow area inside the three support panels served as the measurement chamber for the plate-shaped spent fuel assembly. This design facilitated the efficient detection and measurement of neutrons emitted from the spent fuel assembly, while minimizing interference from external sources.

4.4 Arm and back detector structure

The arm detector is used for detecting fast neutrons generated by the induced fission in spent fuel. Therefore, HDPE was selected as primary support material. HDPE provides structural support, facilitates neutron moderation, and shields against neutron radiation. A ^{3}He counting tube was embedded in the HDPE to detect fission neutrons. When fission neutrons enter the detector, they collide with HDPE to achieve the desired moderating effect. In addition, the HDPE functions as a shield against external neutrons, thereby reducing the impact of environmental background neutrons. Moreover, it prevents fission neutrons generated by spent fuel from escaping and causing radiation damage to personnel.

As illustrated in Fig. 2, cadmium sheets with a specific thickness were added to the two arms of the measurement chamber to absorb the scattered neutrons from the spent fuel at the neutron source. The fission neutron energy spectra passing through the cadmium sheets and entering the arm detectors were simulated with varying cadmium sheet thicknesses (0mm, 1mm, 2mm, and 3mm). The results in Fig. 5 indicate that without cadmium sheets, only the thermal and fast neutrons reached polyethylene. Thermal neutrons originated from moderated source neutrons scattered by the spent fuel, whereas fast neutrons were generated by induced fission in the spent fuel.

When a 1-mm-thick cadmium sheet was added, as shown in Fig. 5(b), 96.54% of the thermal neutrons were absorbed, and the percentage of fast neutrons increased to 98.39%. The

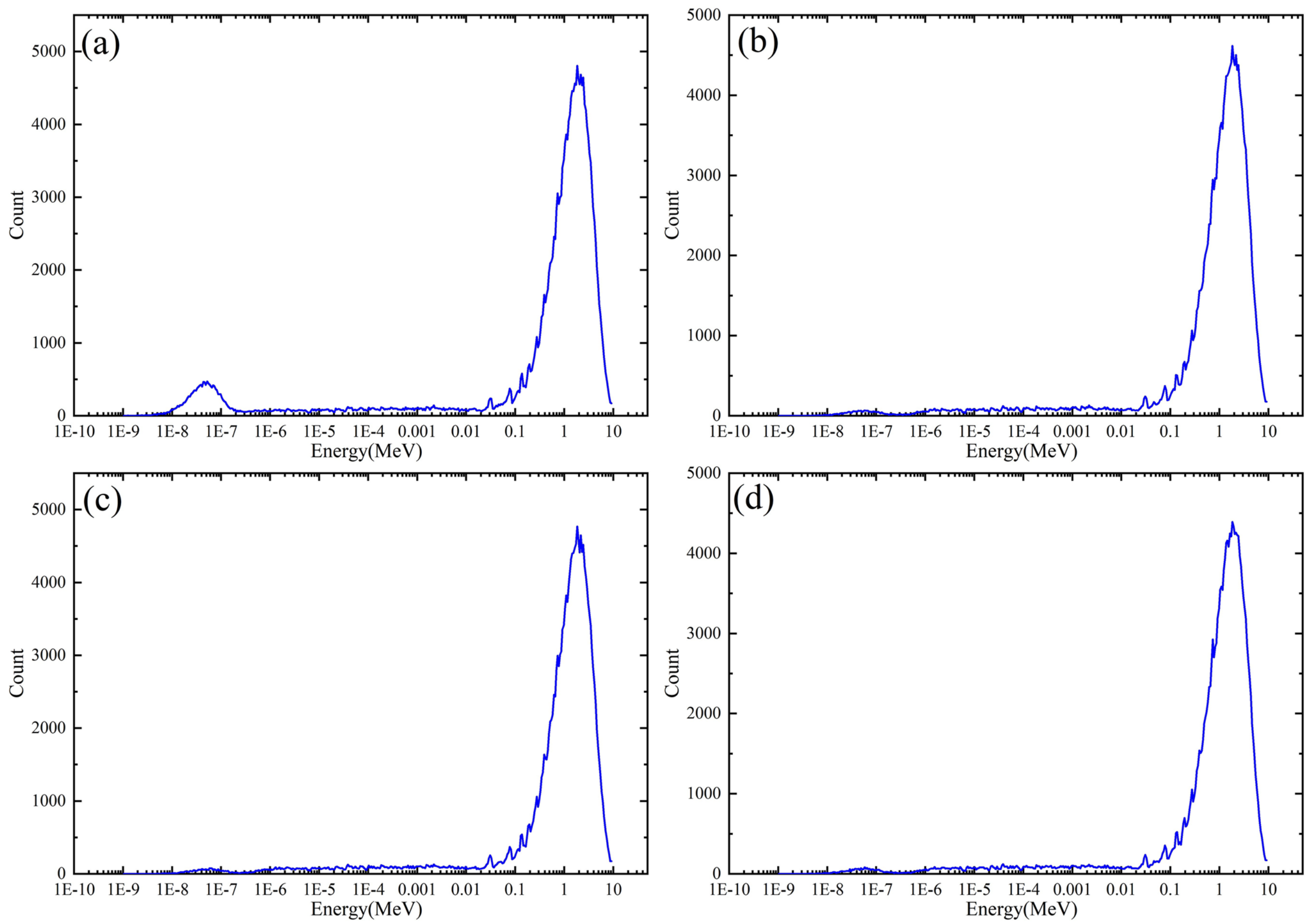

Fig. 5 (Color online) Effect of different thickness of cadmium sheets on the fission neutron energy spectrum: **a** 0 mm; **b** 1 mm; **c** 2 mm; and **d** 3 mm

neutron energy spectrum was minimally affected by increasing the cadmium sheet thickness (Fig. 5(c) and 5(d)). This resulted in the final selection of a 1-mm-thick cadmium sheet for optimal performance. This choice enhanced the efficiency of the arm detector in capturing and detecting fission neutrons, while minimizing interference from other neutron sources.

The primary purpose of the back detector is to detect the unabsorbed transmitted neutrons that pass through the spent fuel assembly. In contrast to the arm detector, the transmitted neutrons experienced moderating effects from both the moderator and the spent fuel assembly. Because the neutrons generated by induced fission are fast neutrons, the support material of the back detector did not need to fulfill the neutron moderation function.

Considering these factors, and with an emphasis on better physical properties, aluminum alloy was chosen as the support body for the back detector. Aluminum alloys are well suited to this role, providing structural support without contributing to the moderating effect of neutrons. This optimized the efficiency of the back detector in capturing and detecting unabsorbed transmitted neutrons, while minimizing unnecessary interference from the support material itself.

After the fundamental modeling of the detector was established, the detection efficiency of the detection system with different geometrical parameters was simulated. The detection efficiency of the neutron detection system is defined as

$$\varepsilon_{\mathrm{a}} = \frac{n_{\mathrm{a}}}{N_{\mathrm{a}}} \times 100\% \quad (1)$$

and

$$\varepsilon_{\mathrm{b}} = \frac{n_{\mathrm{b}}}{N_{\mathrm{b}}} \times 100\% \quad (2)$$

where ε_{a} is the detection efficiency of the arm neutron detection system. ε_{b} is the detection efficiency of the back-neutron detection system. n_{a} is the neutron count recorded by the arm neutron detection system. n_{b} is the neutron count recorded by the back-neutron detection system. N_{a} is the number of neutrons emitted by the assembly to the arm neutron detection system. N_b is the number of neutrons emitted by the assembly and source to the back-neutron detection system.

This study involved varying the thickness of the support plate and the position of the ^{3}He counting tubes to assess their impact on the detection efficiency of the neutron detection system. Specifically, a 30-mm space was reserved between the assembly and detectors on the two arms and back to satisfy the passing requirements and optimize the detection efficiency.

In Geant4 simulations, the thickness of the support plate was set to 80 mm, 90 mm, 100 mm, and 110 mm. The ^{3}He counting tubes were uniformly arranged in the polyethylene plate, with their centers at specific distances from the surface of the support plate close to the component side: 17.19 mm, 22.19 mm, 27.19 mm, 32.19 mm, 37.19 mm, 42.19 mm, 47.19 mm, and 52.19 mm. Individual cases were studied separately. Figure 6a shows the arm detector detection efficiency versus the polyethylene thickness and the ^{3}He detector position, and Fig. 6b shows the back-detection efficiency versus aluminum alloy thickness and ^{3}He detector position. These plots provide insight into the optimal configuration of the detection system by considering various geometrical parameters.

The analysis of Fig. 6a revealed that the detection efficiency of the arm detector increased with the thickness of the HDPE plate. This improvement was attributed to the role of HDPE in moderating the number of fission neutrons. However, the increase in detection efficiency became marginal when the polyethylene plate reached a thickness of 110mm, with an increment of less than 0.6%. To strike a balance between the performance and equipment miniaturization, the final decision was to set the HDPE thickness to 110mm.

Further, for a constant HDPE thickness, the detection efficiency increased and then decreased as the distance between the center of the ^{3}He tube and the edge of the HDPE plate varied. The efficiency peaked at a distance of 37.19 mm. This behavior was explained by the fact that certain fission neutrons, after entering polyethylene, were directly detected by the ^{3}He counting tube at the front end, whereas others were reflected by the polyethylene at the back end and are then detected. Therefore, an optimal detector structure was achieved when the polyethylene at both ends of the ^{3}He counting tube attained an appropriate thickness.

The final size of the HDPE plate was $220\,\text{mm} \times 210\,\text{mm} \times 110\,\text{mm}$, and the center of the ^{3}He counting tube was positioned 37.19 mm from the edge of the HDPE. Under these conditions, the detection efficiency reached a maximum of 21.85%. This configuration strikes a balance between the thickness of the polyethylene plate and the positioning of the ^{3}He counting tube, thereby ensuring the optimal performance of the arm detector.

Figure 6b illustrates the trend of the back-detection efficiency with changes in the geometric parameters of the aluminum alloy plate. Notably, the detection efficiency of the back detector was higher than that of the arm detector. It decreased as the thickness of the support plate increased and as the distance between the ^{3}He counting tube and the inside of the support plate increased. However, the overall trend was not pronounced.

The behavior observed was attributed to the scattering characteristics of aluminum alloy material. Although aluminum alloys scatter thermal neutrons to a certain extent, their scattering ability is lower than that of polyethylene alloys. Consequently, increasing the thickness at the front end resulted in a decrease in the detection efficiency.

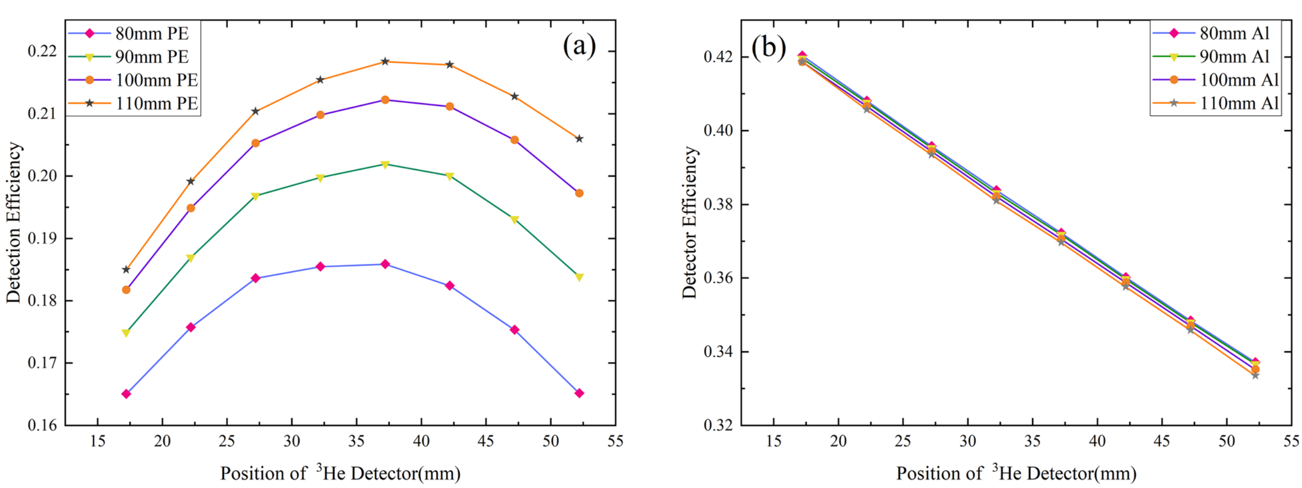

Fig. 6 (Color online) Detection efficiency ε_f versus polyethylene and aluminum plate geometry parameters. **a** Arm detection efficiency. **b** Back detection efficiency

However, a slight increase in the detection efficiency was observed when the thickness of the back end was increased.

After careful consideration, the size of the back detector considered was a 220 mm $\times$ 210 mm $\times$ 110 mm aluminum alloy plate, placing the ^{3}He counting tube close to the inner side of the aluminum alloy plate and leaving only a 5-mm gap at the inner edge. The detection efficiency of the back-detection system reached 42.05%. This configuration ensured a balance between the thickness of the aluminum alloy plate and the positioning of the ^{3}He counting tube, thereby achieving optimal performance for the back detector.

5 Response curves and conclusions

5.1 Neutron spectrum from spent fuel assembly

In this study, source neutrons were initially moderated by a moderator before interacting with the spent fuel assembly. This process involved the emission of neutrons from the spent fuel assembly. The emitted neutrons were subsequently collected using a neutron detection system. The source neutron spectrum used in this study was derived from the spectrum of neutrons obtained after the initial moderation. Therefore, the neutrons emitted from the plate spent fuel assembly comprised two primary components:

Fission neutrons:These are neutrons induced by the fissile nuclides present in the assembly. A sizable number of neutrons are released from fission reactions, and their contribution to the emitted neutron spectrum is a crucial aspect of this analysis.

Source neutron transmission:This term refers to the neutrons that are part of the initial source spectrum and are transmitted through the spent fuel assembly without being subjected to any additional interactions.

The combination of these two components forms the overall spectrum of neutrons emitted from the plate spent fuel assembly, which is essential for the accurate characterization and analysis of the performance of the neutron detection system.

The plate-shaped spent fuel assembly had a height of 600 mm. Considering its elongated structure, a track-based approach was planned for the stepwise measurement of the burnup of the fuel assembly during the actual measurement process. Similarly, a stepwise approach was adopted for the simulation. Specifically, a 100-mm segment of the assembly centered on the neutron source irradiation was selected for the simulation of the emitted neutron field. This focused simulation facilitated a detailed examination of the neutron characteristics in a specific region of the fuel assembly.

In the context of using the arm detector to measure the response relationship between fission neutron counts exiting from the side and the depth of spent fuel burnup, an illustrative example of a plate-shaped spent fuel assembly with a burnup of 30% was considered. The neutron energy spectra of both sides of the assembly are shown in Fig. 7a.

Observation of the spectrum revealed two counting peaks:

• Lower count peak located at 10^{-8} MeV **to** 10^{-7} MeV.

•Higher count peak positioned at 10^{-1} MeV **to** 10 MeV.

This phenomenon was attributed to the presence of source-scattered neutrons in addition to fission neutrons in the emitted neutron spectrum. Source-scattered and fission neutron spectra were obtained on both sides of the assembly (Fig. 7b and c). The key findings of the simulation are as follows:

• The source-scattered neutron spectra closely matched the incident neutron spectra.

• The fission neutron spectrum followed the standard Maxwell-Boltzmann distribution.

These results validate the reliability of the simulation. Notably, fission neutrons emitted from both sides of the module accounted for 86.67% of the total neutron count when the burnup was 10%. This information contributes to understanding the composition of the neutron spectrum and aids in the development of a reliable response relationship for the arm detector in relation to burnup.

The back detector recorded the response relationship between the source-transmitted neutrons emitted by the spent fuel assembly and the burnup. The emitted neutron field was subjected to the same treatment and the resulting (Fig. 7d–f) is analyzed.

Figure 7e shows the source-transmitted neutron energy spectrum. Notably, there was a significant percentage of fast neutrons in the tail compared to the incident neutron energy spectrum. This phenomenon can be attributed to the high cross-section of the thermal neutron reaction owing to the various thermal neutron absorbers contained in the spent fuel assembly materials. Thus, a sizable portion of the thermal composition of the incident neutrons was absorbed by the component. In addition, the fission neutrons produced by the induced fission of thermal neutrons in the fissile nuclides in the assembly also contributed certain fast neutrons.

At a burnup of 30%, 62.53% of the total neutrons were transmitted by the incident neutrons through the assembly. Therefore, most of the neutrons detected by the back detector originated from external neutron sources.

5.2 Neutron counting and spent fuel burnup response model

The relationship between the counts recorded by the arm detector and the burnup response of the spent fuel assembly of the plate section is illustrated in Fig. 8a. As the burnup increased, the counts of the arm detectors gradually decreased, demonstrating a robust linear relationship between the two variables ($R^2 = 0.9601$). This correlation

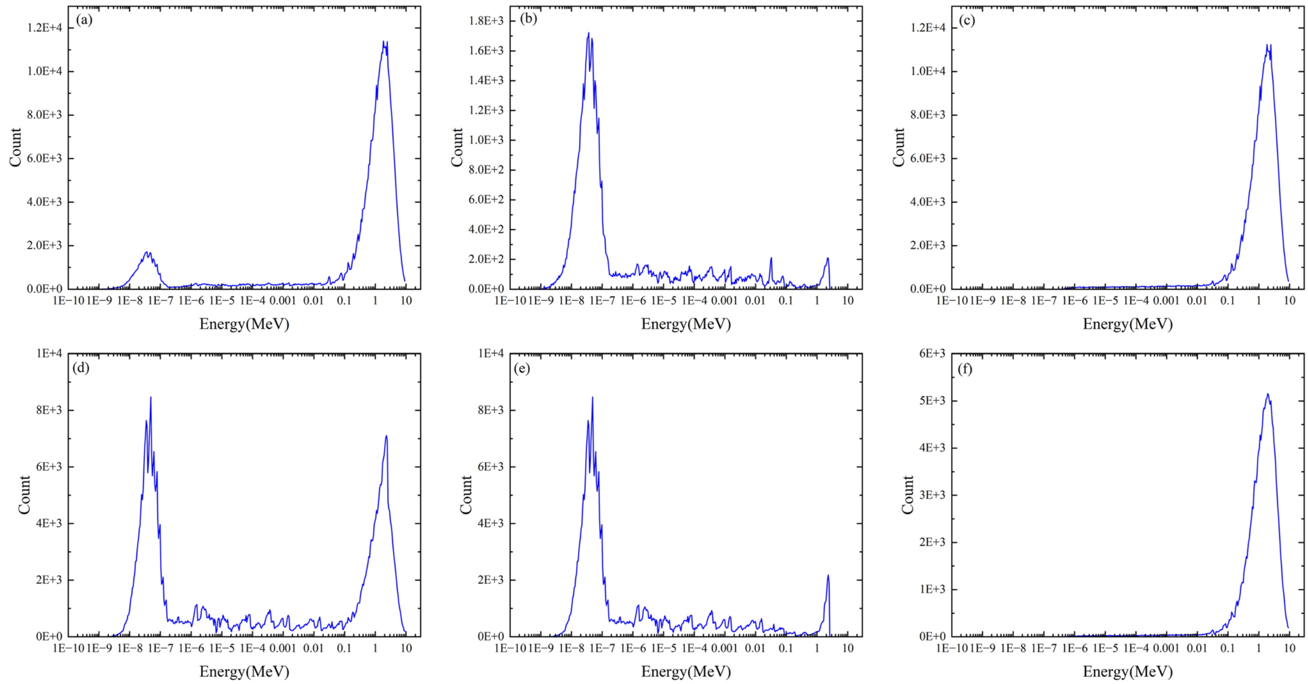

Fig. 7 (Color online) Neutron energy spectrum of plate spent fuel assembly (30% Burnup). **a** Arm total outgoing neutron energy spectrum; **b** arm source scattering neutron energy spectrum; **c** arm fission neutron energy spectrum; **d** back total outgoing neutron energy spectrum; **e** back source scattering neutron energy spectrum; and **f** back fission neutron energy spectrum

can be attributed to the role of the arm detector in detecting the induced fission neutrons. The number of induced fission neutrons was positively correlated with the content of fissile nuclides in the spent fuel. As burnup deepened, the content of fissile nuclides diminished, resulting in a gradual reduction in the number of induced fission neutrons. The resulting response relationship between the arm detector count and burnup is

$$X_a = -467.84BU + 103512.75. \quad (3)$$

where X_a represents the arm detector counts and BU represents the spent fuel assembly burnup in percent fissile nuclide consumption. The formula is applicable to a burnup range of 0–50%. Figure 8b depicts the trend of the ratio of the arm detector counts to the number of emitted fission neutrons with burnup. As evident, the ratio of the arm detector count to the number of fission neutrons emitted from the component stabilized at approximately 0.2082. Furthermore, the fluctuations within the range of 0–50% of burnup did not exceed 0.0022, demonstrating a prominent level of stability. This observation validated the rationality of the design of the detection system.

Figure 8c illustrates the relationship between the back-detector counts and the burnup. In contrast to arm detectors, the counts of back detectors were primarily influenced by neutrons transmitted from the source. The trends shown in Figs. 8c indicated a positive correlation between the back-detector counts and burnup. This correlation can be attributed to the gradual decrease in fissile nuclides in the spent fuel as the burnup increases. In addition, most fission-produced neutrons have a fast neutron composition, contributing less to back detectors without moderating measures. The presence of fission products, particularly neutron poison nuclides, such as Xe and Sm, can also affect the results of the back detector. According to IAEA-TECDOC-233 [36], the amounts of Xe and Sm peaked at 5% of the fuel consumption and then decreased as the burnup increased. This explains why the transmission neutron counts were lower than those of the fresh fuel at a low burnup. As the burnup deepened, the reduction in fissile nuclides and nuclides with large neutron absorption cross sections, such as Xe and Sm, resulted in the relationship shown in Fig. 8c. The results became even more complicated when the effects of additional neutron poisons were considered. The final relationship between the back detector counts and burnup is obtained as follows:

$$X_b = 2024.91BU + 194791.73, \quad (4)$$

where X_b is the back-detector count, BU is the burnup in units of the percentage of fissile nuclide consumption, and $R^2 = 0.9528$.

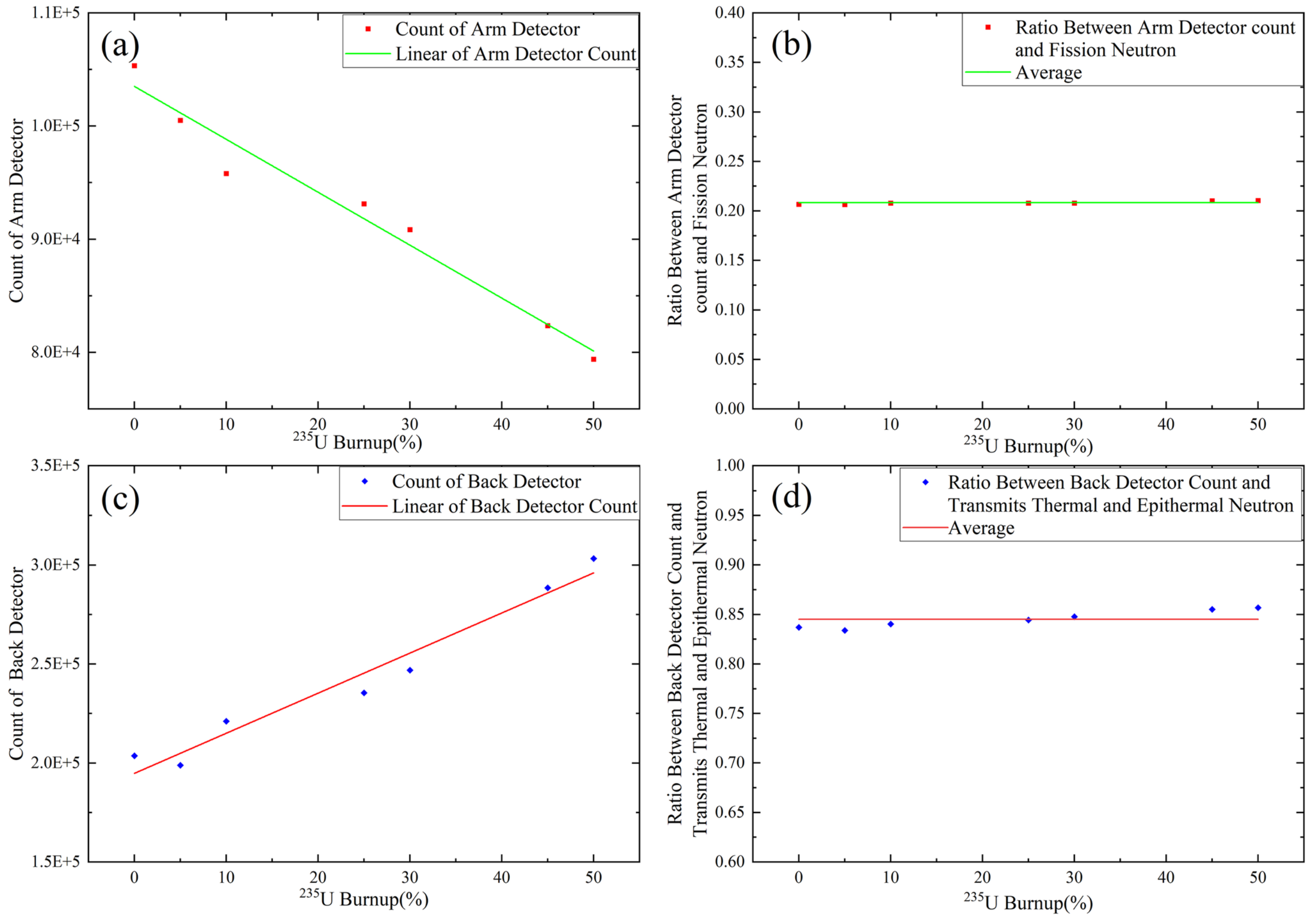

Fig. 8 (Color online) Relationship between the detector and burnup. **a** Relationship between arm detector counts and burnup response; **b** ratio of arm detector counts to outgoing fission neutron counts at different burnups; **c** relationship between back detector counts and burnup response; and **d** ratio of back detector counts to outgoing fission neutron counts at different burnups

The trend of the ratio of the back detector counts to the number of transmitted thermal neutrons with combustion depth is presented in Fig. 8c, d. As evident, the relationship between the back-detector count and number of transmitted thermal neutrons remained stable, with upward and downward fluctuations of no more than 0.012. Figure 8d illustrates that the ratio of the back detector counts to the number of transmitted thermal and epithermal neutrons gradually increased with increasing burnup. This shift resulted from the decreased absorption of transmitted thermal neutrons as burnup increased, leading to a softer transmitted neutron energy spectrum and a change in the average neutron energy from 0.8494 MeV to 0.6159 MeV. Because the cross-section of the reaction between ^{3}He and neutrons is negatively correlated with the neutron energy, a reduction in the average neutron energy results in more detector counts.

The above analysis revealed a robust linear correlation between the arm and back detectors of the “U-shaped” ^{3}He neutron detection system with the burnup of spent fuel assembly. This correlation enabled precise measurements of the quantities of fission and thermal neutrons emitted from the assembly, facilitating the accurate determination of the burnup. Notably, the back detector exhibited superior measurement accuracy compared with the arm detector. In conclusion, the “U-shaped” ^{3}He neutron detection system devised in this study enhanced the precision of the active neutron method for measuring the depletion depth of spent fuel assembly. This was achieved by establishing a relationship among the transmitted thermal neutrons, fission neutrons, and depletion depth through concurrent measurements at the back and arm detectors, providing mutually reinforcing insights.

6 Summary

This study proposed a burnup measurement system for a plate segment spent fuel assembly using a compact D-D neutron generator. The system incorporated a moderator and “U-shaped” measurement equipment, with the optimization of physical and geometrical parameters based on burnup data obtained from the IAEA 10 MW MTR. The D-D neutron generator demonstrated the ability to deliver 5.0×10^8 nps of 2.45MeV fast neutrons. The configured moderator (75 mm PE + 260 mm Al) effectively moderated the fast neutrons to thermal or epithermal neutron, achieving a neutron flux of 3.73×10^{-5} n/cm^2 s^{-1} (per unit source neutron) with a thermal neutron proportion of 74.1%.

The induced fission of fissile nuclides in spent fuel, triggered by thermal neutrons, resulted in the production of fission neutrons. The measurement of the fission and transmission neutron counts exhibited a linear relationship with burnup, with R^2 values of 0.9601 and 0.9528, respectively. The influence of poisoning on the detection results was qualitatively described. In future work, the influences of Xe, Sm, and other neutron poison nuclides on the measurement results will be studied quantitatively.

The findings of this study confirmed the feasibility of the physical design of the burnup measurement system based on the compact D-D neutron generator and demonstrated its capability to accurately measure the burnup of a spent fuel assembly.

Author Contributions All authors contributed to the study conception and design. The Monte Carlo simulation, detector design, data collection, and analysis were performed by Yi-Nong Li, Kang Wu, Zheng Wei, and Xing-Yu Liu. The first draft of the manuscript was written by Yi-Nong Li, and all authors commented on the previous versions of the manuscript. All the authors have read and approved the final version of the manuscript.

Data Availability The data that support the findings of this study are openly available in Science Data Bank at https://cstr.cn/31253.11.sciencedb.j00186.00410 and https://doi.org/10.57760/sciencedb.j00186.00410.

Declarations

Conflict of interest The authors declare that they have no conflict of interest.

References

1. Y.S. Al-Omar, A.A. Mohammad, P. Jongharк et al., Transient thermal hydraulic analysis of the IAEA 10MW MTR reactor during loss of flow accident to investigate the flow inversion. Ann. Nucl. Energy. **62**, 144–152 (2013). https://doi.org/10.1016/j.anucene.2013.06.010
2. S. Dawahra, K. Khattab, G. Saba, Calculation of fuel burnup and radionuclide inventory in the 10MW MTR type research reactor using the GETERA code. Ann. Nucl. Energy. **78**, 89–92 (2015). https://doi.org/10.1016/j.anucene.2015.01.009
3. K.S. Chaudri, S.M. Mirza, Burnup dependent Monte Carlo neutron physics calculations of IAEA MTR benchmark. Prog. Nucl. Energy. **81**, 43–52 (2015). https://doi.org/10.1016/j.pnucene.2014.12.018
4. F. Sakurai, Y. Horiguchi, S. Kobayashi et al., Present status and future prospect of JRR-3 and JRR-4. Phys. Rev. B Condens. Matter Mater. Phys. **311**, 7–13 (2002). https://doi.org/10.1016/S0921-4526(01)01048-1
5. C.T. Ye, China advanced research reactor (CARR): a new reactor to be built in China for neutron scattering studies. Phys. Rev. B Condens. Matter Mater. Phys. **241–243**, 48–49 (1998). https://doi.org/10.1016/S0921-4526(97)00509-7
6. Y. Nakahara, K. Suyama, T. Suzaki, Technical development on burnup credit for spent LWR fuels.(JAERI. Publishing osti.gov, 2000). https://www.osti.gov/etdeweb/biblio/20138179
7. C.V. Parks, M.D. DeHart, J.C. Wagner, Review and prioritization of technical issues related to burnup credit for LWR fuel. (ORNL Publishing, 2000). https://doi.org/10.2172/814192https://www.osti.gov/biblio/814192/. Accessed 25 Dec 2023
8. Y. Socol, Y. Gofman, M. Yanovskiy et al., Assessment of probable scenarios of radiological emergency and their consequences. Int. J. Radiat. Biol. **96**, 1390–1399 (2020). https://doi.org/10.1080/09553002.2020.1798544
9. A.S. Chesterman, *Spent fuel measurements to improve storage and transport efficiency* (KAIF Meeting Spent Fuel Management, South Korea, 2002)
10. B.B. Bevard, J.C. Wagner, C.V. Parks et al., Review of information for spent nuclear fuel burnup confirmation (2009). https://www.nrc.gov/reading-rm/doc-collections/nuregs/contract/cr6998/index.html. Accessed 25 Dec 2023
11. A. Lebrun, G. Bignan, Non-destructive assay of nuclear low-enriched uranium spent fuels for burnup credit application. Ann. Nucl. Energy. **135**, 216–219 (2001). https://doi.org/10.13182/NT01-A3217
12. T.S. Li, D. Fang, Review of burnup measurement methods for nuclear fuel. Nucl. Electron. Detect. Technol. 289–291 (2005). (**in Chinese**)
13. H.M. Jin, D.M. Liu, Non-destructive assay methods for the burn-up measurement of power reactor spent fuel assemblies. At. Energy Sci. Technol. **30**, 185–192 (1996). (**in Chinese**)
14. L.J. Yang, A review of non-destructive burnup measurement methods. Nucl. Electron. Detect. Technol. 148–152 (2011). (**in Chinese**)
15. W.H. Yan, *Research on burnup measurement method and prototype development in high temperature gas cooled reactor* (Tsinghua University, Department of Physics, 2013). **(in Chinese)**
16. S.Q. Zhao, D.Z. Qian, G.B. Wang et al., Gamma spectrum burnup measurement method based on short half-life nuclides. High Power Laser Part. Beams. **29**, 135–139 (2017). https://doi.org/10.11884/HPLPB201729.170165. (**in Chinese**)
17. T.S. Li, D. Fang, H. Li, et al., Burnup measurement of 10MW high temperature gas cooled reactor. Nucl. Electron. Detect. Technol. 129–131 (2006). (**in Chinese**)
18. L. Zhu, G.L. Liu, J.J. Liu, Theoretical research on location of fuel assemblies failure using the activity ratio of ^{134}Cs and ^{137}Cs. Nuclear Tech. **42**, 100602 (2019). https://doi.org/10.11889/j.0253-3219.2019.hjs.42.100602 (**in Chinese**)
19. Y.L. Zheng, J.H. Li, Y.G. Zhao, Application of Monte Carlo method in CZT detector to measure spent fuel assembly burn-up. At. Energy Sci. Technol. **46**, 81–85 (2019). **(in Chinese)**
20. C. Mao, *Study of HTR-10 burnup measurement method based on anti-compton technology* (East China University of Technology, Nuclear science and technology, 2018). **(in Chinese)**
21. International Atomic Energy Agency, *Advances in Applications of Burnup Credit to Enhance Spent Fuel Transportation*, (Storage, Reprocessing and Disposition, Vienna, 2007)
22. X.X. Chen, X.L. Chen, J.C. Zhao et al., Burn-up Distribution Measurement of One Irradiation Test Subassembly in CEFR. At. Energy Sci. Technol. **53**, 1051–1054 (2019). https://doi.org/10.7538/yzk.2018.youxian.0591. (**in Chinese**)
23. B. Yan, C.Y. Liu, C.B. Dai, Optimization design of on-line burnup measurement system for high temperature gas cooled

reactor. Nucl. Electron. Detect. Technol. **35**, 1154–1158 (2015). (**in Chinese**)
24. T. Ma, B. Xia, J.L. Wang et al., Error analysis and experimental research of HTR-10 burn-up measurement system based on MCNP modeling. Sci. Technol. Rev. **30**, 25–28 (2012). https://doi.org/10.3981/j.issn.1000-7857.2012.20.002. (**in Chinese**)
25. M.L. Dong, B.T. Tong, C.H. Zhang, Fork detector for non-destructive measurement of spent fuel assemblies. At. Energy Sci. Technol. **03**, 59–64 (1998). ((**in Chinese**))
26. R.D. Li, A.V. Bushyev, A.F. Korin, The determination of ^{235}U content and burnup in spent fuel assemblies in reactors is studied. Nucl. Power Eng. **30**, 56–59 (2009)
27. H.F. Dou, R.D. Li, S.L. Zhu et al., Determination of fissile nuclide ^{235}U content in re-irradiated spent fuel assemble with nondestructive assay. Nucl. Power Eng. **39**, 51–55 (2018). https://doi.org/10.13832/j.jnpe.2018.03.0051
28. X.Y. Liu, Design study of burn-up depth measurement system for the plate-shaped spent fuel based on compact D-D neutron generator. (School of Nuclear Science and Technology, Lanzhou University, 2023)
29. D. Henzlova, H.O. Menlove, C.D. Rael et al., Californium interrogation prompt neutron (CIPN) instrument for non-destructive assay of spent nuclear fuel-Design concept and experimental demonstration. Nucl. Instrum. Methods Phys. Res. Sect. A **806**, 43–54 (2016). https://doi.org/10.1016/j.nima.2015.09.089
30. A.C. Trahan, G. E. McMath, P. M. Mendoza et al., Results of the Swedish spent fuel measurement field trials with the differential die-away self-interrogation instrument. Nucl. Instrum. Methods Phys. Res. Sect. A **955**, 163329 (2020). https://doi.org/10.1016/j.nima.2019.163329
31. H. Trellue, G. McMath, A. Trahan et al., Spent fuel non-destructive assay integrated characterization from active neutron, passive neutron, and passive gamma. Nucl. Instrum. Methods Phys. Res. Sect. A **988**, 164937 (2021). https://doi.org/10.1016/j.nima.2020.164937
32. S. Agostinelli, J. Allison, K. Amako et al., Geant4-a simulation toolkit. Nucl. Instrum. Methods Phys. Res. Sect. A **506**, 250–303 (2003). https://doi.org/10.1016/S0168-9002(03)01368-8
33. J. Allison, K. Amako, J.E.A. Apostolakis et al., Geant4 developments and applications. IEEE Trans. Nucl. Sci. **53**, 270–278 (2006). https://doi.org/10.1109/TNS.2006.869826
34. Y.Y. Zhong, X.F. Zhou, CrossSection transport correction methods for material test reactor MTR benchmark. Modern Appl. Phys. **14**, 103–109 (2023). https://doi.org/10.12061/j.issn.2095
35. K.S. Chaudri, S.M. Mirza, Burnup dependent Monte Carlo neutron physics calculations of IAEA MTR benchmark. Prog. Nucl. Energy. **81**, 43–52 (2015). https://doi.org/10.1016/j.pnucene.2014.12.018
36. P.J. Russell, D.C. Sammon. Research reactor core conversion from the use of highly enriched uranium to the use of low enriched uranium fuels. guidebook addendum: Heavy water moderated reactors. (IAEA Publishing, 1985). https://doi.org/10.1016/S0921-4526(97)00509-7
37. Z.W. Huang, J.R. Wang, Z.W. Ma et al., Design of a compact D-D neutron generator. Nucl. Instrum. Methods Phys. Res. Sect. A **904**, 107–112 (2018). https://doi.org/10.1016/j.nima.2018.07.005
38. W. Wang, J.R. Wang, Z.P. Li et al., Design and implementation of control system for compact DD neutron generator. Nuclear Tech. **39**, 050402 (2016). https://doi.org/10.11889/j.0253-3219.2016.hjs.39.050402
39. X.Y. Liu, X.X. Yu, H.Z. Li et al., Physical design of conversion screens for thermal neutron transmission imaging. Nucl. Tech. **46**, 110203 (2023). https://doi.org/10.11889/j.0253-3219.2023.hjs.46.110203. (**in Chinese**)
40. Z.M. Hu, C.Q. Liu, Z.W. Ma et al., Simulation and design of fast neutron sensitivity silicon microchannel plate. Nucl. Tech. **45**, 020201 (2022). https://doi.org/10.11889/j.0253-3219.2022.hjs.45.020201. (**in Chinese**)
41. Z.Q. Guo, C.Q. Liu, W.Z. Zhang et al., Optimization design of BNCT neutron source and moderating body based on accelerator $^{7}Li(p, n)$ reaction. Nucl. Tech. **45**, 050201 (2022). https://doi.org/10.11889/j.0253-3219.2022.hjs.45.050201. (**in Chinese**)